Subsurface rock interface imaging with the application of Ground Penetrating Radar (GPR)

Zijian Li, Yingjian Xiao, Rick Pigrim, Justin Royce, Stephen Butt
Drilling Technology Lab (DTL) of Memorial University of Newfoundland, St. John's, NL, Canada

ABSTRACT
In this study, ground penetrating radar (GPR) data were collected in field trials both on the surface and downhole. The target of this study is to evaluate the possibility of the identification of the rock interface between gold ore and surrounding rock using borehole GPR. The basic theory of GPR was reviewed before the trials. In surface field trials, the GPR data were collected to identify the rock interface between shale and limestone in a quarry and to identify the rock interface between basalt and rhyolite in cripple bay. In the downhole field trials, the GPR antenna was put in the borehole in the mining site. The GPR imaging result was analyzed with the consideration of the field geometries. Then, the penetration depth and the ability to identify the subsurface structure was evaluated. According to the result, GPR units with the center antenna frequency of 1GHz presents a smaller penetration depth than 250MHz GPR, which is 2.5m for surface imaging in homogenous material and 1.8m for downhole imaging. Primary reflections are collected in the results and concur with the field geometries. This study also revealed some problems. The fast traveling speed of the antenna reduced the noise cancelling efficiency and influenced the imaging quality. Unexpected reflections found in the result, which may be a result of a lack of understanding of the field geometry. Overall, 1GHz GPR showed its potential in the downhole imaging application and further work should be done to improve the quality and accuracy.

RÉSUMÉ
Dans cette étude, les données du radar de pénétration au sol (GPR) ont été collectées lors d'essais sur le terrain en surface et en fond de trou. L'objectif de cette étude est d'évaluer la possibilité d'identifier l'interface entre la roche entre le minerai d'or et la roche environnante à l'aide du forage GPR. La théorie de base de GPR a été examinée avant les essais. Lors d'essais au champ en surface, les données GPR ont été collectées pour identifier l'interface entre le schiste et le calcaire dans une carrière et pour l'interface entre le basalte et la rhyolite dans la baie estropiée. Dans les essais de terrain en fond de trou, l'antenne GPR a été placée dans le forage du site minier. Le résultat de l'imagerie GPR a été analysé en prenant en compte les géométries de champ. Ensuite, la profondeur de pénétration et la capacité à identifier la structure du sous-sol ont été évaluées. Selon le résultat, les unités GPR avec une fréquence d'antenne centrale de 1 GHz présente une profondeur de pénétration inférieure à celle du 250 MHz GPR, soit 2,5 m pour une imagerie de surface dans un matériau homogène et 1,8 m pour une imagerie en fond de trou. Les réflexions primaires sont collectées dans les résultats et concordent avec les géométries de champ. Cette étude a également révélé certains problèmes. La vitesse de déplacement rapide de l'antenne réduisait l'efficacité de la suppression du bruit et influençait la qualité de l'image. Des réflexions inattendues dans le résultat peuvent être le résultat d'un manque de compréhension de la géométrie du champ. Dans l'ensemble, le GPR 1GHZ a montré son potentiel dans l'application d'imagerie en fond de trou et des travaux supplémentaires devraient être menés pour améliorer la qualité et la précision.

1. INTRODUCTION

Ground penetrating radar (GPR) is a popular geophysical imaging technique used for infrastructure imaging, such as soil moisture, archeology and downhole imaging. GPR emits electromagnetic (EM) waves and the delineates the structure using the received echo which is reflected and differentiated by the change of material EM properties. The GPR is an ultra-wideband (UWB) EM wave device which uses a broad range of frequency of 10–5000 MHz and gains its popularity by numerous advantages. For example, the GPR system acquires and processes the signal in real time, and the result can be presented while operation is ongoing. When different EM wave frequencies are used, the resultant spatial scale ranges from kilometers to centimeters. In addition, GPR is a non-destructive testing (NDT) method which brings no damage to the material.

The adoption of GPR come into existence in the field of geoscience after the mid-1950s (El Said, 1956; Waite and Schmidt, 1961). After 2000, the application of GPR mushroomed due to the development of digital computation and processing ability. Then, the application expanded to more research fields and larger scale imaging practice (Annan, 2002; Bristow and Jol, 2003). Francke et al. (2012) used GPR for the exploration of mineral resources to a large scale. Zaki et al. (2018) used GPR to detect the cavity in karst topography for tunnel construction.

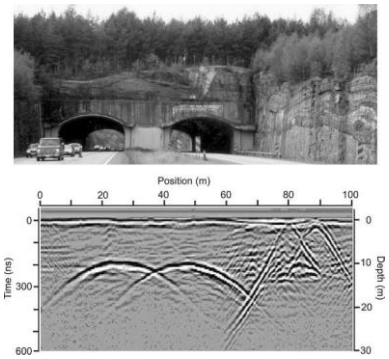

Figure 1. Ground penetrating radar (GPR) cross section obtained with a 50-MHz system traversing over two road tunnels.

In the Sustainable Mining while Drilling (SMD) project, the gold ore vein is thin and tilted with a dip angle around 70 degrees from horizontal, which increases the difficulty of the ore development. The SMD concept aims at a low dilution, high-efficiency mining process, in which a high-resolution geography imaging method is required. In this study, the target is to evaluate the possibility of the identification of the rock interface between gold ore and surrounding rocks using borehole GPR.

Application of borehole GPR started in the 1970s after the invention of downhole antennas. At first, the target of the borehole GPR is to characterize the fractures, cavity, and property changes in the rock mass for nuclear waste disposal (Olsson, 1987; Olsen, 1992). Then Gilson et al. (1996) used GPR for a smaller scale hydrogeological test [153] . Gregoire et al. (2006) used GPR to check the steam-enhanced remediation in fractured limestone in a time-lapse mode. Mansour et al. analyzed the hydraulic property of the fracture subsurface structure using GPR. Serzu et al. (2006) used GPR to map the natural fracture distribution in the granitic bedrock. Dang et al. (2018) used ultra-wideband borehole GPR detected downhole geometries and proved its accuracy.

In this study, both laboratory and field experiments are conducted to evaluate the possibility of the borehole GPR to delineate the interface between the surrounding rocks and the gold ore. In the laboratory tests, the influence of water and plastic case on signal quality are evaluated. In field trials, the GPR is tested both along the ground surface and downhole to test its maximum imaging depth and the ability to image the rock face.

2. BACKGROUND

The EM properties (ε , μ , σ) dictate EM wave transmission and reflection in the material. Generally, the variations in permittivity ε and conductivity σ are most important while variations in electron mobility μ are seldom discussed. Ground penetrating radar is most useful in low-electrical-loss materials where the penetration depth is increased. Generally, clay content, saline water, and conductive metal are the main influence factors on the penetration depth. Based on Maxwell equations, the penetration depth β is derived for low-electrical-loss materials.

$$f(\beta,t) \approx f(\beta \pm vt)e^{\mp\alpha\beta} \quad [1]$$

Where,

$$v = \frac{1}{\sqrt{\varepsilon\mu}} \quad [2]$$

$$\alpha = \sqrt{\frac{\omega\mu\sigma}{2}}\ if\ \omega\varepsilon \ll \sigma \quad [3]$$

or

$$\alpha = \frac{1}{2}\sigma\sqrt{\frac{\mu}{\varepsilon}}\ if\ \sigma \ll \omega\varepsilon \quad [4]$$

There, v, α and ω are velocity, attenuation coefficient and wave frequency, respectively. It is noticed that the penetration depth has a negative correlation with the material conductivity and the wave frequency.

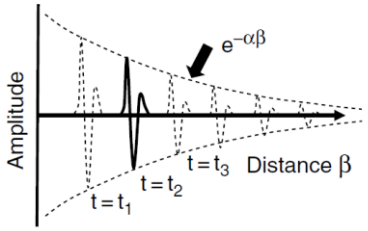

Figure 2. EM wave propagates and decays in amplitude with the distance

When the incident EM waves are emitted and arrive at an material interface, a part of them will reflect back and others will transmit through this interface to the other medium. Partition of reflected and through-transmitted EM waves can be described using the following reflection and transmission coefficients.

$$R = \frac{\text{Reflected Amplitude}}{\text{Incident Amplitude}} = \frac{\sqrt{\varepsilon_1}-\sqrt{\varepsilon_2}}{\sqrt{\varepsilon_1}+\sqrt{\varepsilon_2}} \quad [5]$$

$$T = \frac{\text{Transmitted Amplitude}}{\text{Incident Amplitude}} = \frac{2\sqrt{\varepsilon_2}}{\sqrt{\varepsilon_1}+\sqrt{\varepsilon_2}} \quad [6]$$

It is observed that the magnitude of reflected EM waves is dependent on the permittivity difference of rocks about the interface.

The radial and lateral resolution of the GPR is calculated as:

$$\Delta r \geq \frac{Wv}{4} \quad [7]$$

$$\Delta l \geq \sqrt{\frac{Wvr}{2}} \quad [8]$$

Where Δr represents radial resolution and Δl represents lateral resolution; W is the half period of the GPR wave; r is the distance to the target. It is concluded that the resolution is mainly dictated by the wave velocity and the wave frequency.

3. EXPERIMENT INSTRUMENTS

The capability of the GPR systems is tested in this study. The Noggin 1000 MHz GPR unit from Sensors and Software Inc. is used in this study as shown in Figure 3, which includes a GPR unit, a display, a control panel, battery and data storage. The GPR unit is 30cm long by 15cm wide and 12cm high. The GPR system is protected in a 3D printed plastic case when used in downhole survey as shown in Figure 4.

Figure 3. 1GHz Noggin GPR unit

Figure 4. Downhole survey with GPR unit protected

The data acquired by the Noggin 1000 MHz is collected using the Digital Video Logger (DVL) from Sensors and Software Inc. Then the data is post processed using EKKO Project software. The Noggin 1000 MHz has a center frequency of 1000 MHz and a minimum sampling step size of 0.5cm. The Noggin's sampling step size is primarily dependent on the scanning depth and the stacking number. In the laboratory experiment and the surface imaging field trials, the minimum sampling step size is used while the stacking number is adjusted by the DVL automatically.

4. GROUND SURFACE FIELD TRIAL

4.1 Field trial in CBS quarry

The GPR field survey is conducted in Conception Bay South Quarry B, Quarry F and cripple bay. In these sites, transitions between shale and limestone, red shale and igneous rock and Basalt and Rhyolite are observed. In these tests, shale represents a multiple layered rock material through which the EM attenuation is higher than homogeneous material; the transition from Basalt and Rhyolite is regarded as an analogy to the transition from the gold vein (quartz) to mafic volcanic. The surficial geology conditions are shown in Figure 5, 6 and 7.

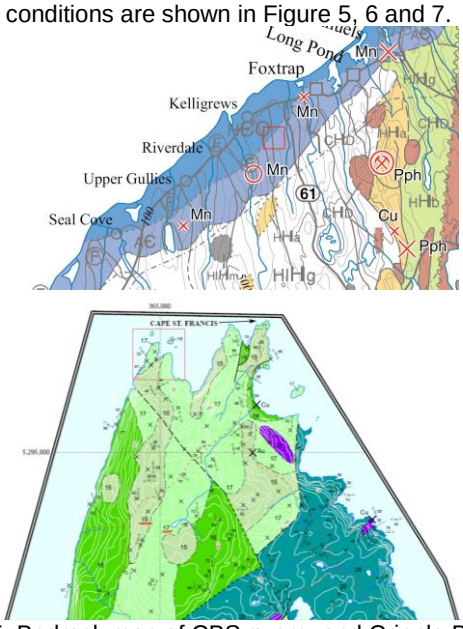

Figure 5. Bedrock map of CBS quarry and Cripple Bay

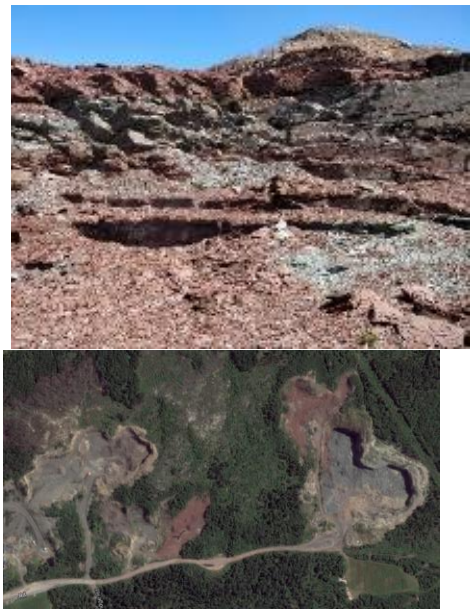

Figure 6. Surficial geology condition of CBS Quarry

Figure 7. Surficial geology condition of Cripple Bay

In the field trial in the Quarry, a 250 MHz GPR unit is also used. Then the results of 250MHz GPR and 1GHz GPR are compared. More than 50 data sets in total are collected and analyzed. Typical results are further discussed below. As shown in Figure 8, two data sets for the same geometry collected by different GPR units are compared. The upper chart is the result from the 250MHz GPR while the lower chart is from the 1GHz GPR. The total

distance of this line view is 72m. In this line, the antenna crossed a transition boundary from shale to limestone. During survey on shale and limestone, a maximum penetration depth of about 3.5 m is obtained from the 250MHz GPR unit, while the maximum penetration depth is about 0.8 m from the 1GHz GPR. It is consistent with the theoretical prediction that the maximum penetration depth decreases with the increasing EM wave frequency. In terms of radial resolution, however, that of 250MHz GPR (around 15cm) is about four times larger than that of 1GHz GPR (around 4cm), which agrees with the theoretical calculation.

The result of this line view shows that the layered material such as shale greatly influences the GPR penetration depth. Specifically, the 1GHz GPR is not suitable for layered material imaging due to great attenuation in wave amplitudes.

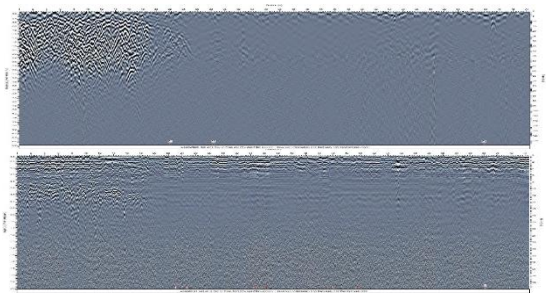

Figure 8. Line view result comparison between 250MHz GPR (upper) and 1GHz GPR (lower) in CBS quarry

4.2 Field trial in Cripple Bay

In Cripple Bay, only 1GHz GPR is used in the Basalt and Rhyolite transition region. These two rocks are homogeneous with no obvious fractures, which is a similar condition to the mining site. Also, the rock interface between them can be found on the surface, which is used as a reference in the surface line view. One typical result is shown in Figure 9. In this line view, a pinch-out of Basalt is observed at the beginning at a penetration depth of around 1.2m. The reflection of the interface between basalt and Rhyolite is very clear. Penetration depth in rhyolite (right) also reaches 2.5m in this survey, without the energy loss through the rock interface. This result shows that the 1GHz GPR has a good penetration depth in homogeneous materials.

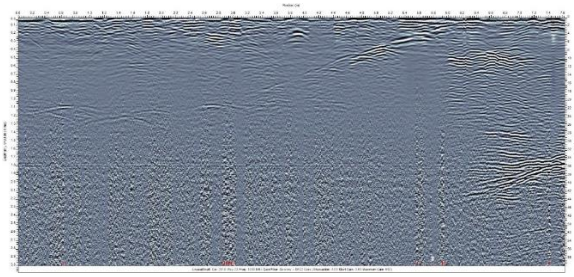

Figure 9. Line view result of 1GHz GPR (lower) in CBS quarry: transition from Basalt to Rhyolite

5. DOWNHOLE FIELD TEST

5.1 Geometry introduction

In the downhole field test, two 10m deep vertical boreholes with ~9in diameters are tested which are drilled in the ore zone of Romeo & Juliet Vein. The gold ore vein is quartz, while the surrounding rock is Mafic Volcanic as shown in Figure 10.

Figure 10 Surrounding rock of Mafic Volcanic (a), gold ore quartz (b) and a small layer of Volcanic stone (c) mixed in the vein (from cutting analysis)

A quartz vein outcrop is used as a reference for the hole drilling. The thickness of the vein is around 4m while the dip angle is around 70 degrees (20 degrees from vertical). Hole No.1 is located at 1.65m away from the vein outcrop while hole No.2 is drilled in the middle of the vein, as shown in Figure 14. The outcrop and the hole preparation are shown in Figure 11 below. The total depths of both holes are around 10m. In field GPR survey, the survey along boreholes reaches the depth of approximately 6m due to the limitation of the length of the data transmitting cable.

Figure 11. Test hole drilling near the vein outcrop

Then, using these two holes, the downhole GPR tests are conducted. Different antenna tool face angles are tested due to that the GPR antenna is shielded, meaning EM waves will be emitted and received at specific direction. For Hole #1, when the GPR is facing perpendicular to the rock interface and moving upwards, the distance between the rock interface and the GPR increases from 0m to 1.65m. When the GPR antenna is facing parallel to the vein strike, no rock interface is expected to be shown in the radargrams. However, the reflection in the borehole may reduce the directional imaging capability. The data quality, however, is influenced by the surface reflection of the wellbore and the directional capability of the antenna.

The antenna is protected in a plastic case which is non-conductive. It is hoisted by an electric winch when it works in the hole. The GPR is triggered by time because the wheel for odometer brings difficulties to the waterproof design. The data is collected by a specific time interval which is calculated based on the antenna traveling speed and the step size of 1cm. The antenna is travelling from bottom to surface to finish one survey.

5.2 Data processing and interpretation

The test result of hole #1 and hole #2 are shown in figure 12 and 13 respectively.

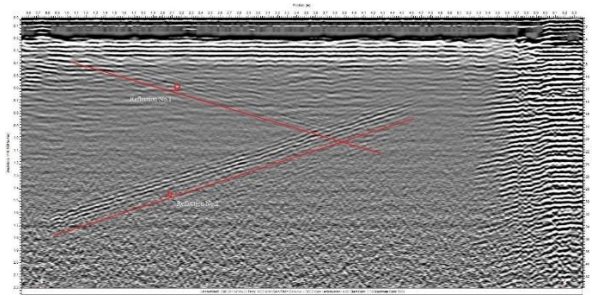

Figure 12. The downhole GPR test result in Hole #1

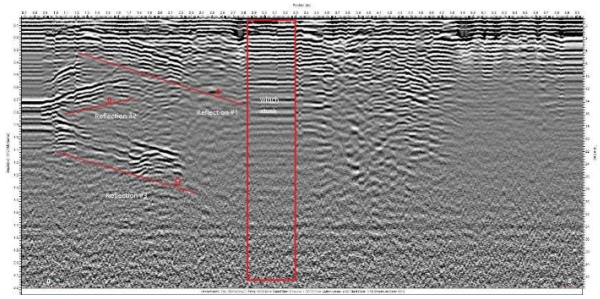

Figure 13. The downhole GPR test results in Hole #2

There are two primary reflections found in figure 12 denoted as #1 and #2. The reflection 1 occurs at around 0.3m away from the borehole center at the beginning; then its penetration depth increases with the antenna traveling upward. When the penetration depth reaches 1.1m after traveling about 4.3m upward, the reflection overlaps with reflection #2 and becomes too weak to distinguish. Reflection #2 start at 1.7m in penetration depth at the beginning and ends at 0.7m of penetration depth after traveling 4.6m upwards. Referring to the underground geometry, reflection #1 agrees well with the interface between the hanging wall and the vein. However, this reflection is non-distinguishable after the antenna finishes survey after 4.3m. Generally, reflection #2 is strong and clear to be shown in the radargram. However, this reflection is not expected because no corresponding geometry has been discovered yet. It is assumed that reflection #2 comes from a rock interface which lies outside the vein.

There are three primary reflections shown in figure 13 which are denoted as #1, #2 and #3. Reflection #1 occurs ~0.3m away from the center of borehole #2 from the starting of survey and then goes further away from the borehole center. Reflections #2 and #3 both exist initially at around 0.8m away from the borehole center. Then, the penetration depth of reflection #2 decreases while that of reflection #3 increases as the survey is moving upwards. Referring to the underground geometry, reflection #1 agrees well with the boundary between the vein and the footwall rock in geometry, with an increase of penetration depth from zero. Then, the penetration depth of Reflection #2 decreases with the antenna is traveling upward, which is not relevant to any known geometry. Reflection #3 is parallel to reflection #1 with about 0.8m in distance. It is assumed that the reflection corresponds to a small reflector such as a layer inside the vein. In addition to these primary reflections, small reflections are also observed in radargram obtained from Hole #2. It is also assumed that these small reflections correspond to small layers in the vein. This assumption is supported by the fact that the quartz vein is mixed with other stone layers known from the cutting analysis after drilling the hole.

In both holes, multiple horizontal reflections are firstly observed in the downhole GPR radargrams which are borehole reverberations. This is generated by the gap between the antenna face and the wellbore wall. Overall, the imaging quality or resolution can be improved by decreasing the speeding of moving antenna along the borehole, which increases the stacking number with a higher signal-noise ratio. Unexpected reflections are observed for both holes.

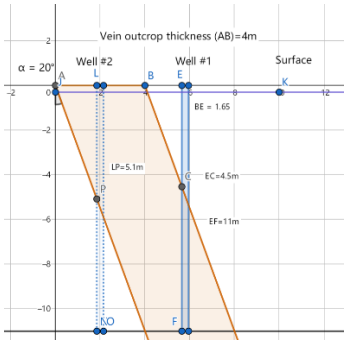

Figure 14. Underground geometry of hole #1 and #2

6. CONCLUSIONS AND RECOMMENDATIONS

In this study, GPR data were collected from surface and downhole field trials. A 1GHz GPR unit is used to evaluate its possibility of the identifying rock interfaces between gold ore (quartz) and surrounding rocks (volcanic mafic) in downhole imaging test. The penetration depth reaches around 2m in downhole condition. In surface field trials, the GPR data were collected to identify the rock interface between shale and limestone in a quarry and that between basalt and rhyolite in Cripple Bay. The GPR results are compared with the actual geometries on site. It is concluded that the penetration capability of GPR is weakened when fractured media is encountered such as shale. Through homogeneous media (rhyolite), the penetration depth reaches a maximum of 2.5m. The interface of basalt and rhyolite is also delineated clearly in the result. The 250MHz GPR is also used in the trial and its result is compared with that from 1GHz GPR. The result shows that the 250MHz GPR unit has an greater penetration depth but worse resolution than that of 1GHz GPR unit. In addition, the 250MHz GPR unit has an larger size than the 1GHz GPR unit. This requires more space for the 250MHz GPR in downhole imaging.

Underground borehole imaging is conducted using 1GHz GPR. Two holes are drilled at the mining site through the host volcanic mafic and the gold ore quartz. The GPR antenna is hoisted and moved along the hole. The imaging is conducted at a series of azimuths. Then the result is analyzed referring to the actual geometry. There are

primary reflections found in the result which concur with the actual rock interface in the testing site. The image quality is not satisfactory because the wave signal gets weaker until it is not distinguishable. Also, the reflection is not consistent in the radargram. Reasons are given as follows. Firstly, the natural fractures and multiple layers in the target formation cause a great attenuation in EM wave amplitudes. Secondly, the GPR antenna moving speed is high, which limits the stacking number of the data acquisition. Thus, noise interference is much more than expectation. A reflection in radargram matches the local geometry of rock interface, while some strong reflections are found and do not correspond any geometry. It is assumed that these reflections represent some rock interfaces or small layers which have not been discovered yet.

Based on the field trial results and the analysis, we believe that the 1GHz GPR shows potential in the downhole imaging. Primary reflection shows 1.8m penetration depth, which is generally satisfactory. There are primary reflections found to concur with the interface between the quartz gold ore vein the volcanic mafic host rock. While there are some issues to be solved in the future. For example, there are some unexpected reflections collected in the field trials. It is recommended that more geotechnical and geological studies should be done before the imaging survey. The image quality is not satisfactory enough due to the limitation of the field equipment. It is suggested that the antenna traveling speed should be small enough to guarantee a high stacking number and thus a high noise-signal ratio. Multiple surface reflections are observed in the images at shallow depth. The algorithm could be improved to remove the surface reflections in the post process.

7. ACKNOWLEDGEMENT

I would like to thank Dr. Stephen Butt for his guidance all over my program. I also would like to express my appreciation to Dr. Allison Leitch for her selfless guidance and devotion to this research. Thank to Anaconda Mining Inc. and MITACS for their support in many ways.

8. REFERENCES

Annan, A.P., 2002, The history of ground penetrating radar. Subsurface Sensing Technologies and Applications, Vol. 3, No. 4, October 2002, pp. 303–320.

Bristow, C.S. and Jol, H.M., 2003, Ground Penetrating Radar in Sediments, Geological Society, London, Special Publications, 211.

Dang, L., Yang, H., & Teng, B. (2018). Detection imaging of impulse borehole well-logging radar. EURASIP Journal on Image and Video Processing, 2018(1), 105.

El-Said, M. A. H. (1956). Geophysical prospection of underground water in the desert by means of electromagnetic interference fringes. Proceedings of the IRE, 44(1), 24-30.

Francke, J. (2012). A review of selected ground penetrating radar applications to mineral resource evaluations. Journal of Applied Geophysics, 81, 29-37.

Gilson, E. W., Redman, J. D., Pilon, J., & Annan, A. P. (1996, January). Near surface applications of borehole radar. In Symposium on the Application of Geophysics to Engineering and Environmental Problems 1996 (pp. 545-553). Society of Exploration Geophysicists.

Gregoire, C., Joesten, P. K., & Lane Jr, J. W. (2006). Use of borehole radar reflection logging to monitor steam-enhanced remediation in fractured limestone—Results of numerical modelling and a field experiment. Journal of applied geophysics, 60(1), 41-54.

Mansour, K., Basheer, A. A., Rabeh, T., Khalil, A., Eldin, A. E., & Sato, M. (2014). Geophysical assessment of the hydraulic property of the fracture systems around Lake Nasser-Egypt: In sight of polarimetric borehole radar. NRIAG Journal of Astronomy and Geophysics, 3(1), 7-17.

Olsson, O., Falk, L., Forslund, O., Lundmark, L., & Sandberg, E. (1992). Borehole radar applied to the characterization of hydraulically conductive fracture zones in crystalline rock 1. Geophysical prospecting, 40(2), 109-142.

Olsson, O., Falk, L., Sandberg, E., Forslund, O., & Lundmark, L. (1987). Crosshole investigations-Results from borehole radar investigations (No. STRIPA-TR--87-11). Swedish Nuclear Fuel and Waste Management Co.

Serzu, M. H., Kozak, E. T., Lodha, G. S., Everitt, R. A., & Woodcock, D. R. (2004). Use of borehole radar techniques to characterize fractured granitic bedrock at AECL's Underground Research Laboratory. Journal of Applied Geophysics, 55(1-2), 137-150.

Zaki, N. F. M., Ismail, M. A. M., Abidin, M. H. Z., & Madun, A. (2018, April). Geological Prediction Ahead of Tunnel Face in the Limestone Formation Tunnel using Multi-Modal Geophysical Surveys. In Journal of Physics: Conference Series (Vol. 995, No. 1, p. 012114). IOP Publishing.